Hindawi
Advances in Meteorology
Volume 2019, Article ID 4381438, 13 pages
https://doi.org/10.1155/2019/4381438

Research Article

Month-to-Month Variability of Autumn Sea Ice in the Barents and Kara Seas and Its Relationship to Winter Air Temperature in China

Chuhan Lu,[1] **Kaili Li**,[1] **Shaoqing Xie**,[2] **Zhaomin Wang**,[3] **and Yujing Qin**[1]

[1]*Key Laboratory of Meteorological Disaster, Ministry of Education, Joint International Research Laboratory of Climate and Environment Change, Collaborative Innovation Center on Forecast and Evaluation of Meteorological Disasters, Nanjing University of Information Science & Technology, Nanjing 210044, China*
[2]*Jiashan Meteorological Bureau, Jiaxing 314100, China*
[3]*College of Oceanography, Hohai University, Nanjing 210000, China*

Correspondence should be addressed to Yujing Qin; qinyujing@nuist.edu.cn

Received 27 May 2019; Revised 30 August 2019; Accepted 29 October 2019; Published 12 December 2019

Academic Editor: Alastair Williams

The variation of autumn Arctic sea ice is a critical indicator of temperature anomalies over the Eurasian continent during winter. The retreat of autumn Arctic sea ice is typically accompanied by negative anomalous winter temperatures over the Eurasian and North American continents. However, such sea ice temperature linkages notably change from month to month. The variation of the autumn Arctic sea ice area and the relationship between the month-to-month sea ice and winter temperature anomalies in China are investigated using the Hadley Centre's sea ice dataset (HadiSST) and the European Centre for Medium-Range Weather Forecasts (ECMWF) reanalysis dataset (ERA-Interim) during 1979–2018. We present the following results: The sea ice in the Barents and Kara seas (BK) during the autumn and winter seasons shows notable low-frequency variability. The retreat of sea ice in the BK from September to November is significantly associated with negative temperature anomalies in the following winter in China. However, the linkage between the sea ice in the BK in September and the winter temperatures is stronger than that in both October and November. An anomalous positive surface pressure is exhibited over the northwestern part of Eurasia in the winter that is linked to decreasing sea ice in the BK in the preceding September. This surface pressure favors the persistence and intensification of synoptic perturbations, such as blocking highs and surface cold highs, as well as the intensification of the Siberian High and the East Asian winter monsoon. These favorable conditions ultimately contribute to the formation of large-scale winter cold anomalies in China. Compared to low sea ice cover in October and November, a more oceanic heat storage in the upper BK induced by low sea ice cover in the BK leads to a larger heat release to tropospheric atmosphere in winter by surface heat flux and upward longwave radiation in the BK. This regional tropospheric warming results in a higher barotropic positive height anomaly over the Ural Mountains, and then more active cold advection from the high latitude affects East Asia.

1. Introduction

Arctic sea ice is a prominent indicator of global climate change. A substantial loss of ice and a higher warming rate have been observed in the Arctic during recent decades, a phenomenon known as Arctic amplification, with a continuous increase in the global air temperature [1]. Severe cold events and anomalously heavy snowfalls have frequently affected most midlatitude regions of the Northern Hemisphere (NH), including major industrialized centers [2, 3]. Along with this unforeseen cooling trend in the midlatitude regions of the NH, both the Cold Siberian High and the East Asian winter monsoon exhibit a substantial decadal intensification, leading to more active cold air outbreaks in China [4, 5]. Recent studies documented that there may be some physical linkages between the recent reduction of ice in the Arctic Ocean and cooling in the midlatitude continents of the NH through the anomalous atmospheric circulation response of sea ice loss [6]. For example, a reduction in the Arctic sea ice is typically

accompanied by substantial warming that weakens the meridional temperature gradient. This will decelerate the westerlies in the midlatitudes and result in a decrease in atmospheric baroclinicity and a more wavy circulation [7, 8]. Compared with the direct response within the troposphere, stratospheric response to sea ice forcing also plays a robust role in the development of cold conditions over midlatitude continents of the NH [9]. There is still a debate regarding the physical connection between the changes in Arctic sea ice and the midlatitude activity of planetary waves [10]. A change in the dominant mode of extratropical circulation may also have a close association with the recent cooling trend [11–13].

Previous studies have shown that extratropical impacts depend highly on the regional structure of the anomalous Arctic climate state [14]. For example, warming over the BK region can lead to East Asian cooling, whereas northern North America cooling is closely related to warming over the East Siberian Sea–Chukchi Sea region [14]. The reduction of sea ice over the BK also has a cooling effect on the European region induced by more blockings associated with the loss of sea ice in the BK [15]. However, atmospheric responses to the sea ice variations of the BK vary with background atmospheric states and seasons. A recent study had pointed out that the loss of sea ice in the BK in November links with a weaker SH in November, while a stronger SH in December [16].

Many previous studies have focused on the relationship between the variations in Arctic sea ice and atmospheric circulation patterns and the associated anomalous climate in China. Xie and Huang [17] reported that changes in Arctic sea ice and sea surface temperature (SST) anomalies in the central and eastern equatorial Pacific play important roles in the general circulation and suggested that there may be physical connections between them. Wu et al. [18] confirmed that the variations in the areas of sea ice in the Greenland Sea and BK are associated with the occurrence of El Niño-Southern Oscillation (ENSO) events and that a 3-year leading signal of anomalous sea ice shows a close linkage with the general circulation in the NH. A numerical simulation also indicated that the variation in Arctic sea ice is one of the most important indicators of an East Asian summer monsoon climate anomaly [19]. Shi et al. [20] documented that there is a positive correlation between the zonal temperature gradient of the Arctic Ocean and the geopotential height gradient between the Barents Sea and the East Siberian Sea at 500 hPa and that the associated anomalous circulation links with the summer precipitation anomalies over Northeast China. Wang et al. [21] also reported that the preceding autumn loss of Arctic sea ice favors a northward shift of the cyclone track in China along with the weakening of Rossby waves over the area south of 40°N in eastern China, resulting in an intensification of haze weather.

The influences of changes in Arctic sea ice on the wintertime air temperature in China under the background of Arctic amplification have drawn extensive attention from scholars in recent years. A series of studies showed that the preceding reduction of Arctic sea ice in autumn, such as the reduction that occurs east of the Arctic Ocean and the BK, is associated with substantial surface warming. A weakening polar/midlatitude temperature gradient results in a Eurasian (EU) pattern response that facilitates the strengthening of the Siberian High and the East Asian winter monsoon, which brings substantial cooling and more extreme low events in East Asia [22–24]. Li et al. [25] documented the local responses of the temperature in East Asia to changes in sea ice in different regions. They reported that the retreat of the sea ice in the BK induces an intensification of the Siberian High and lowers the temperature in the area north of East Asia, while an increase in sea ice in the Okhotsk Sea induces a northerly shift of the jet stream in the upper troposphere over East Asia with substantial warming in the area south of East Asia. The variations of the sea ice in the BK are associated with the Arctic Oscillation (Arctic Dipole pattern) by inducing cross-Arctic-like (Eurasian) teleconnection wave-train patterns that lead to an intensification of cold surge activity in China [26]. The SST anomalies in the NH and the changes in Arctic sea ice were involved in the interdecadal changes in the winter surface air temperature (SAT) over East Asia that occurred approximately during the mid-1990s [4, 27].

It is worthy to note that the variation of the sea ice cover shows clear seasonal and regional dependencies [28], in spite of a general decrease trend of the Arctic sea ice. Furthermore, the relationships between wintertime SAT anomalies in China and sea ice variation in different time scales or regions also display notable diversity [23, 29]. Therefore, we will study the association of month-to-month variability of the regional Arctic sea ice cover in the preceding autumn with the SAT anomalies and its possible linking pathway.

2. Data and Methods

2.1. Data. The data used in this study include the following: (1) the European Centre for Medium-Range Weather Forecasts (ECMWF) reanalysis dataset (ERA-Interim) from 1979 to 2018 is used for deriving data on the daily and monthly air temperatures, sea-level pressure, geopotential height, and horizontal wind with a $2.5^\circ \times 2.5^\circ$ horizontal resolution [30]; (2) monthly mean sea ice concentrations are derived from the Met Office Hadley Centre's sea ice and sea surface temperature (HadiSST 1.1) dataset [31]; (3) the monthly mean heat content is derived from the vertical average of potential temperature (109.8 m above; 11 levels) from the ECMWF ocean reanalysis system ORAS4 [32]; and (4) observed monthly mean surface air temperatures (SATs) are from the National Climate Center of China, including 160 stations.

2.2. Circulation Indices. The definitions of circulation indices are as follows: The westerly index is defined as the differences in the geopotential heights between 40°N and 65°N and between 0° and 122°E [33]. The blocking high frequency is derived from the anomalous 500 hPa midlatitude geopotential height [34]. The anticyclone intensity

over Eurasia is the seasonal mean of the center pressure for each surface high in 6 hourly SLP field during the winter [2]. The regional mean of the SLP (40°N–60°N, 70°E–120°E) represents the intensity of the Cold Siberian High [33], and the East Asian winter monsoon index is defined by the midlatitude land-sea pressure differences between 110°E and 160°E [35]. In addition, the monthly Arctic Oscillation (AO) index (http://www.cpc.ncep.noaa.gov/products/precip/CWlink/daily_ao_index/ao.shtml) can be downloaded from the NOAA Climate Prediction Center (CPC).

3. Variability and Linear Trend of the Arctic Sea Ice

To show the horizontal distribution of the Arctic sea ice, the standard deviation (σ) of the sea ice concentration data from September to December from 1979 to 2018 is shown in Figure 1. Large value areas generally extend from the interior Arctic to the high-latitude oceans in the NH and suggest large interannual variability of the sea ice cover in the marginal areas of the Arctic sea ice. However, clear local characteristics are shown in the above large values of σ areas. In particular, large variability of sea ice occurs in the 70°N–80°N region of the Barents, Kara, and Beaufort seas in September and October (Figures 1 and 1(b)). The northwest coast of Canada and the east coast of Greenland also display high σ values. As a continuous southward expansion of the ice cover, the areas of high σ shift from the preceding Laptev and Beaufort seas to the Bering Sea and the northeast coast of Canada after November (Figures 1(c) and 1(d)). It should be noted that there is a continuous large variability in the BK from September to December. Since the change in sea ice results from strong sea ice-atmosphere coupling, high σ values in the BK indicate that the interannual/interdecadal variation of sea ice in this region may be related to notable changes in atmospheric and oceanic interactions under the background of Arctic amplification [36]. In addition, the variation of the sea ice in the BK can be a good indicator of the East Asian winter monsoon [24]. To understand the effect of sea ice variability on the winter air temperature variability in China, we used the time series of the sea ice cover area over the BK (box area in Figure 1) as the sea ice index (BKI) in this key region.

The original and detrended time series of the BKI, hereafter referred to as the OBKI and DBKI, respectively, during September-October-November (SON) from 1979 to 2018 are presented in Figure 2. The pronounced retreat of autumn sea ice in the BK during the past 40 yrs is indicated by the OBKI in Figures 1(a)–1(c) with values of $-0.81 \times 10^5\,\mathrm{km^2}\cdot 10\,\mathrm{yr^{-1}}$(September), $-1.36 \times 10^5\,\mathrm{km^2}\cdot 10\,\mathrm{yr^{-1}}$ (October), and $-1.19 \times 10^5\,\mathrm{km^2}\cdot 10\,\mathrm{yr^{-1}}$ (November), which are all statistically significant exceeding 0.01. The different decreasing trends of the BKI in the autumn may be because the Arctic sea ice areas in different months correspond to dissimilar general circulations [34]. The remarkable retreat of autumn sea ice in the BK is evident after 2005, which is consistent with the accelerated decrease in the area of Arctic sea ice over the last decade [35]. In addition, the simultaneous correlation coefficients of the OBKI with the Arctic sea ice area index (ASI (downloaded from NSIDC (http://nsidc.org/data/g02135.html))) in September, October, and November are 0.43, 0.55, and 0.47, respectively, which are statistically significant with significance exceeding 0.05. These significant correlations are suggestive of the consistency of the low-frequency sea ice variations between our defined BK region and the Arctic. The DBKI time series shows distinct differences from the OBKI time series during heavy and light ice cover years (defined as $\pm$ 0.75 σ), as indicated in Figures 2(d)–2(f). Additional heavy (light) ice cover years occur before (after) the mid-1990s in the OBKI time series that bear an important decreasing feature. A further discussion of different associations between the OBKI and the DBKI is presented in the following section.

4. Relationship between the Sea Ice and the Air Temperature

Both the OBKI and the DBKI exhibit positive correlations with the wintertime SAT anomalies in most parts of China, as shown in Figure 3, despite their inconsistent time evolutions. As documented in Figures 3(a)–3(c), there are significant positive correlations between the OBKI and the SAT in North China. This is indicated by a cold anomaly likely followed by a preceding autumn sea ice loss in the BK, which is in agreement with the previous studies by Wu et al. [22, 24]. However, the extent of the association decreases from September to November. In particular, significant correlations can be observed over Xinjiang and Northeast China; the largest area is observed in September, after which it shrinks gradually in October and November. The composite differences of the SAT between the low and high OBKI years also show a correlated consistency. In September, low sea ice likely induces a decrease in the SAT in North China, with maximum decreases occurring especially below −1.6°C. In addition, slight cooling is also evident in Southwest China. The correlation patterns in October and November are similar to the September one with a slight reduction of the number of stations with statistical significance.

Stronger associations of the DBKI with the SAT in China in the autumn are observed in Figures 3(d)–3(f), and the month-to-month correlation variations also decrease similar to the association of the OBKI with the SAT. In September, pronounced areas of larger significance are observed over most of China compared with the OBKI (73.8% stations with significance exceeding 0.05), except for the Tibetan Plateau and its vicinity (Figure 3(d)). The composite differences in the SAT between low and high DBKI years are generally −0.8°C in the significant regions. The significant results described above represent a good indication of the variation of the sea ice in the BK in September when compared with the SAT in China in the following winter. In October, significant SAT anomaly regions are observed in Xinjiang, Northeast China, North China, and the Changjiang-Huaihe River Basin, which decreases in size in November similar to Northeast China.

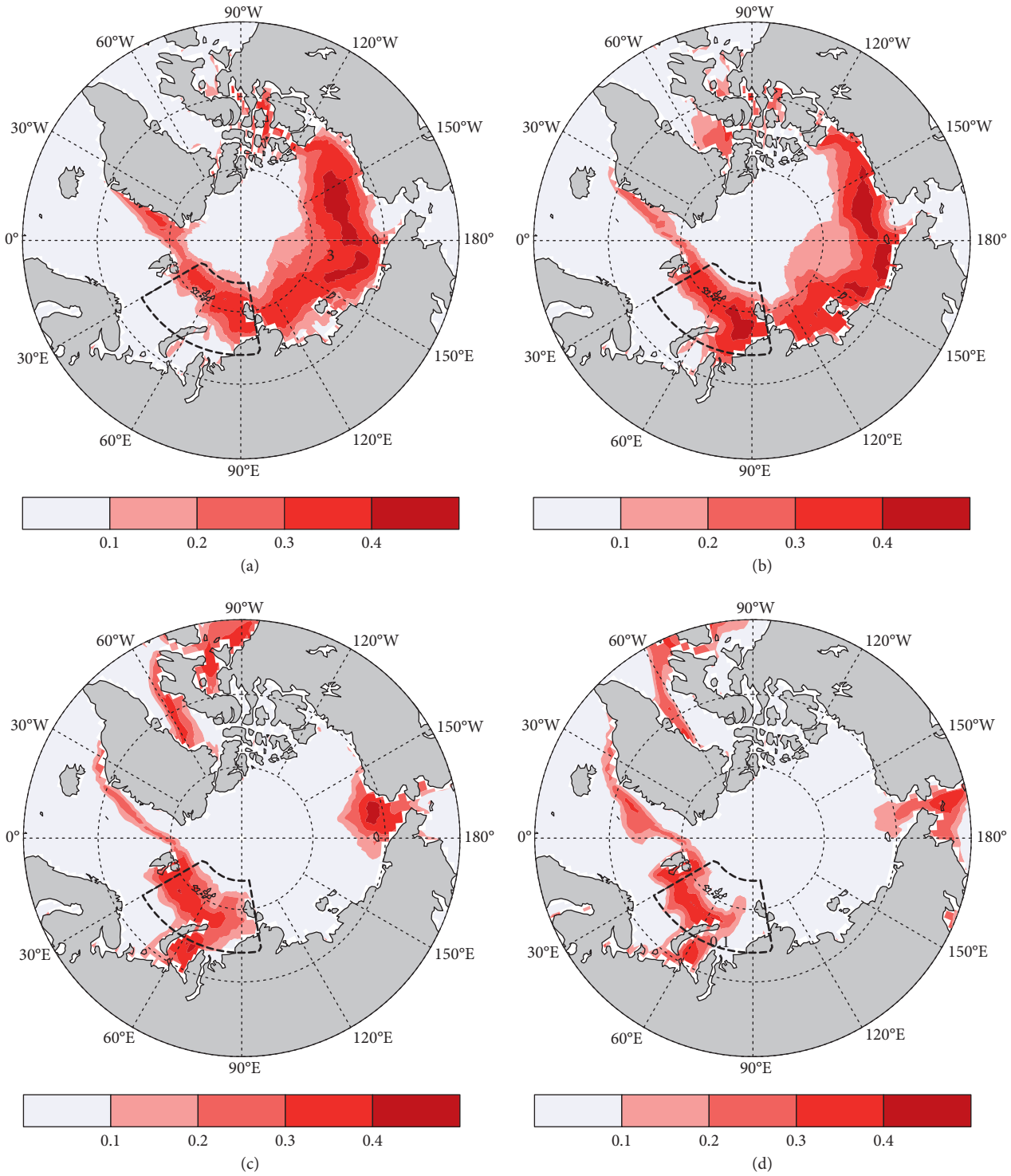

Figure 1: Standard deviations of the Arctic sea ice concentration data for September (a), October (b), November (c), and December (d) from 1979 to 2018. The black dashed box denotes the Barents Sea and the Kara Sea region.

To further study the relationship between the sea ice and the SAT, we conducted an empirical orthogonal function (EOF) analysis for the station SAT anomalies in the winter. The variance contribution rates for the first two modes are 50.7% and 19.3%, which can be well defined according to the criterion proposed by North et al. [37]. The spatial distribution of the leading mode (EOF1) and its corresponding time series (PC1) are shown in Figures 4(a) and 4(c). The EOF1 mode shows a pattern of consistent positive SAT departures in most of China (except the Tibetan Plateau) with a general north-to-south decrease in SAT values. This indicates either consistent cooling or consistent warming of China in the winter. A comprehensive analysis using EOF1 and PC1 indicates that a dominant cooling trend emerged in

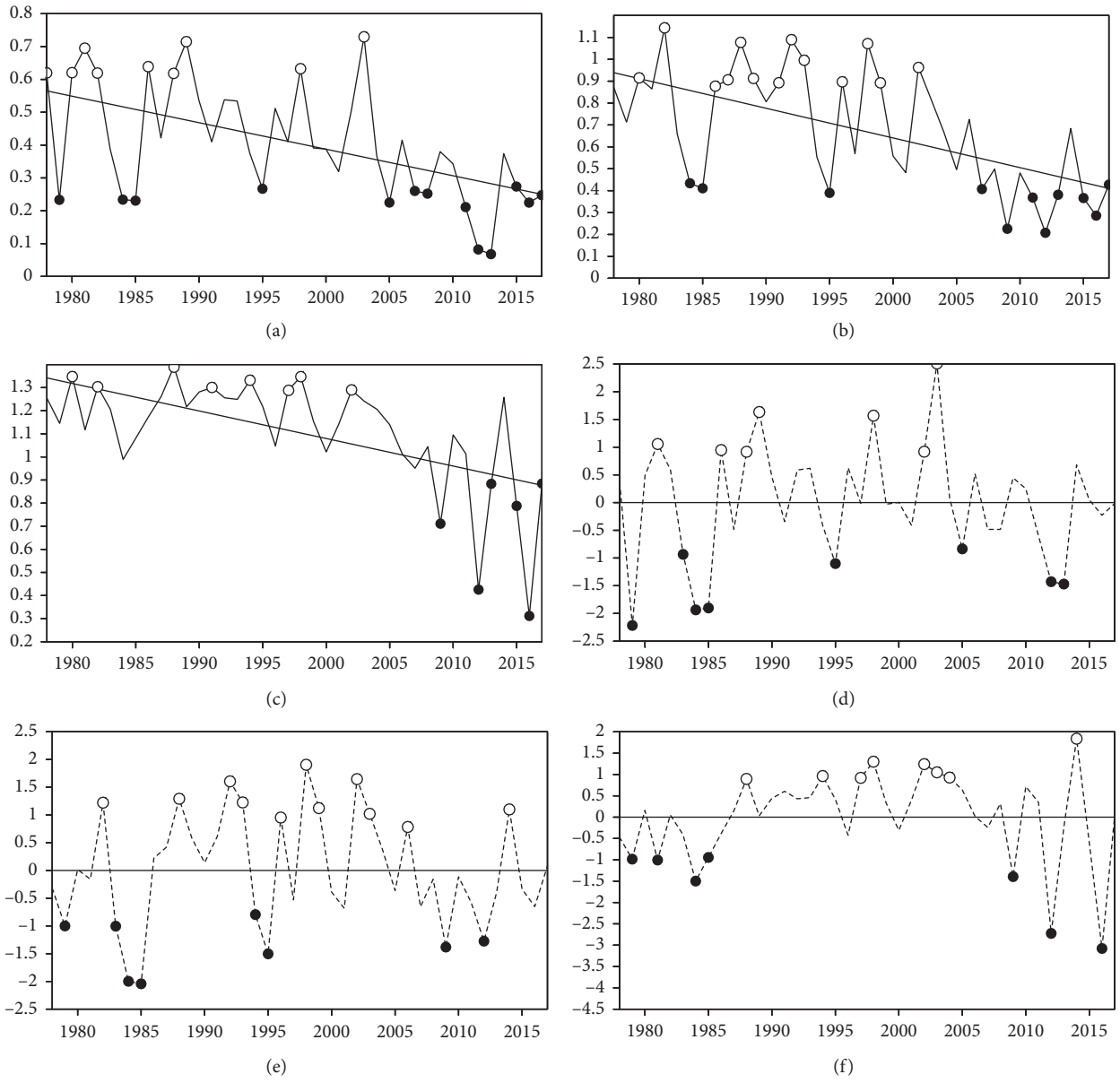

Figure 2: BKI time series for September (a, d), October (b, e), and November (c, f) showing the time series of both the OBKI in the left panels (unit: 10^5 km^2) and the DBKI in the right panels. The straight lines in the left panels denote the linear trends in the OBKI. Those years with high BKI values (>0.75 SD) and low BKI values (<−0.75 SD) are marked by circles and black dots, respectively.

the mid-1980s and after 2010, while a prominent warming trend was dominant in the late 1980s and 2000s with a larger SAT departure amplitude in the northern part of China. In addition, a notable interannual fluctuation can be observed since the late 1990s which is confirmed by a wavelet analysis that shows a substantial 2- to 4-year fluctuation since the early 21st century (figure not shown).

To further assess the correlation between the SAT principal component and the sea ice variation, the correlation coefficients between the month-to-month OBKI, DBKI, ASI, and PC1 and PC2 were calculated, the results of which are documented in Table 1. The difference between the month-to-month OBKI and DBKI is statistically significant with significance exceeding 0.01. Moreover, significant positive correlations between the OBKI, DBKI, and PC1 are evident, and the correlation between the DBKI and PC1 is clearly higher than that between the OBKI and PC1. A notable correlation decrease is evident from September to November. Particularly, the correlation coefficient between the DBKI in September and PC1 is 0.48 with significance exceeding 0.01, while the correlation between the DBKI and PC1 in November decreases to 0.19. The significant correlations between the sea ice in the BK and PC1 further suggest that the change in the sea ice in the BK in the autumn can be utilized as a skillful predictor of the winter SAT anomalies in China, especially for the DBKI in September. However, similar decreases in the correlations between the ASI and PC1 are evident, and the original ASI also shows a lower

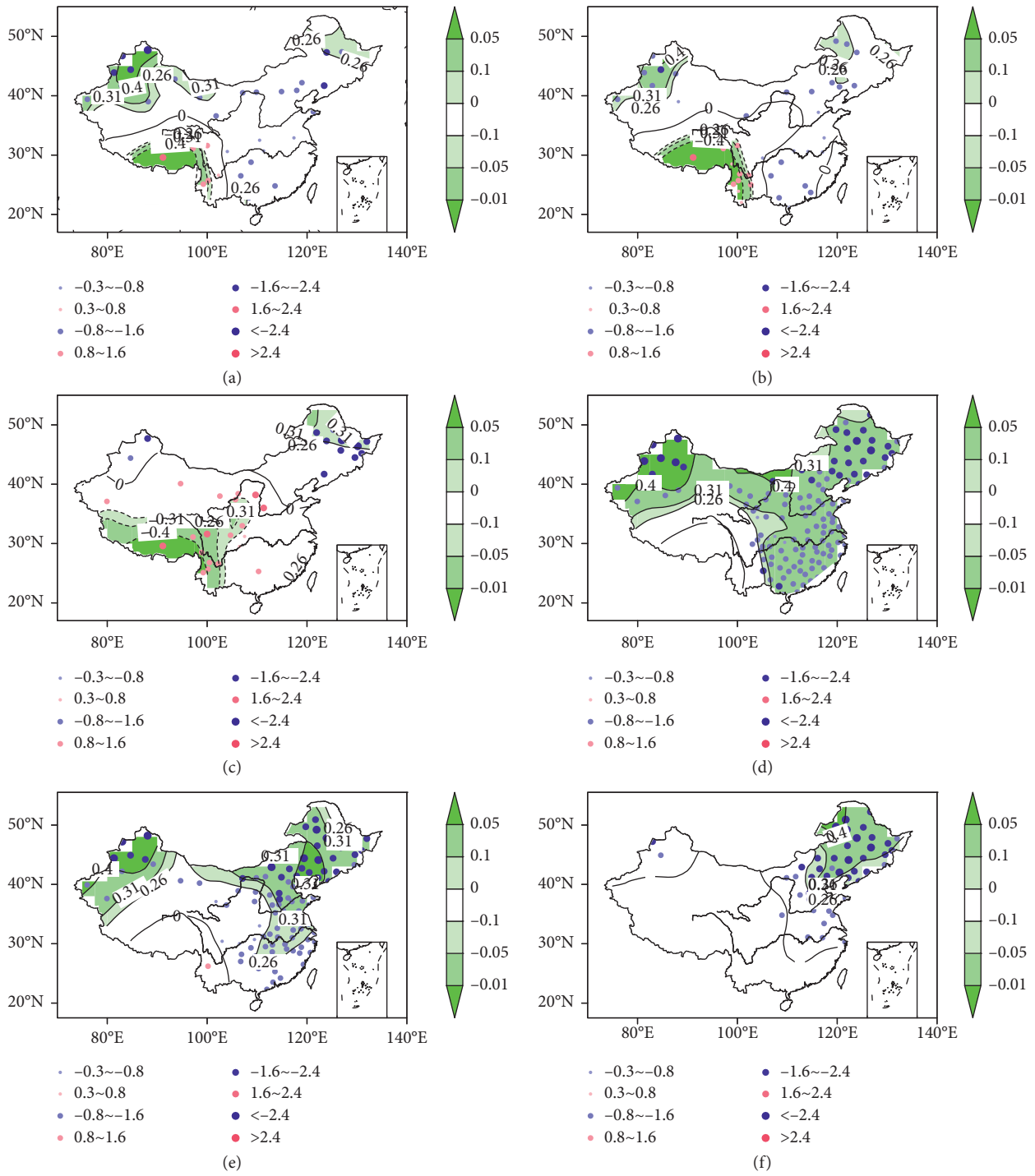

Figure 3: Correlation coefficients between the BKI for September (a, d), October (b, e), and November (c, f) and the winter (DJF) temperature time series for 160 stations in China (shaded: significance and contour: correlation coefficient values) and the composite differences in the temperatures (dots; unit: ˚C) between selected low BKI years and high BKI years. The upper panels are for the OBKI, and the bottom panels are for the DBKI. Both the shaded areas and the dots indicate values that are statistically significant with significance exceeding 0.1 based on the results of *t*-tests. The values in the color bar represent the significance levels of the *t*-test.

positive correlation with the SAT than the detrended ASI. Comparatively, the correlation between the ASI and the SAT is notably lower than the correlation between the BKI and PC1. This implies that the BK is the key region in the Arctic in which the change in the sea ice cover may play a critical role in the winter SAT anomalies in China.

EOF2 is characterized by an opposite variation between Northeast China and the other regions in China (Figure 4(b)). The persistent positive value of PC2 suggests a cold anomaly in the western and southern parts of China before the late 1990s, resulting in warmer conditions in these areas. However, neutral positive

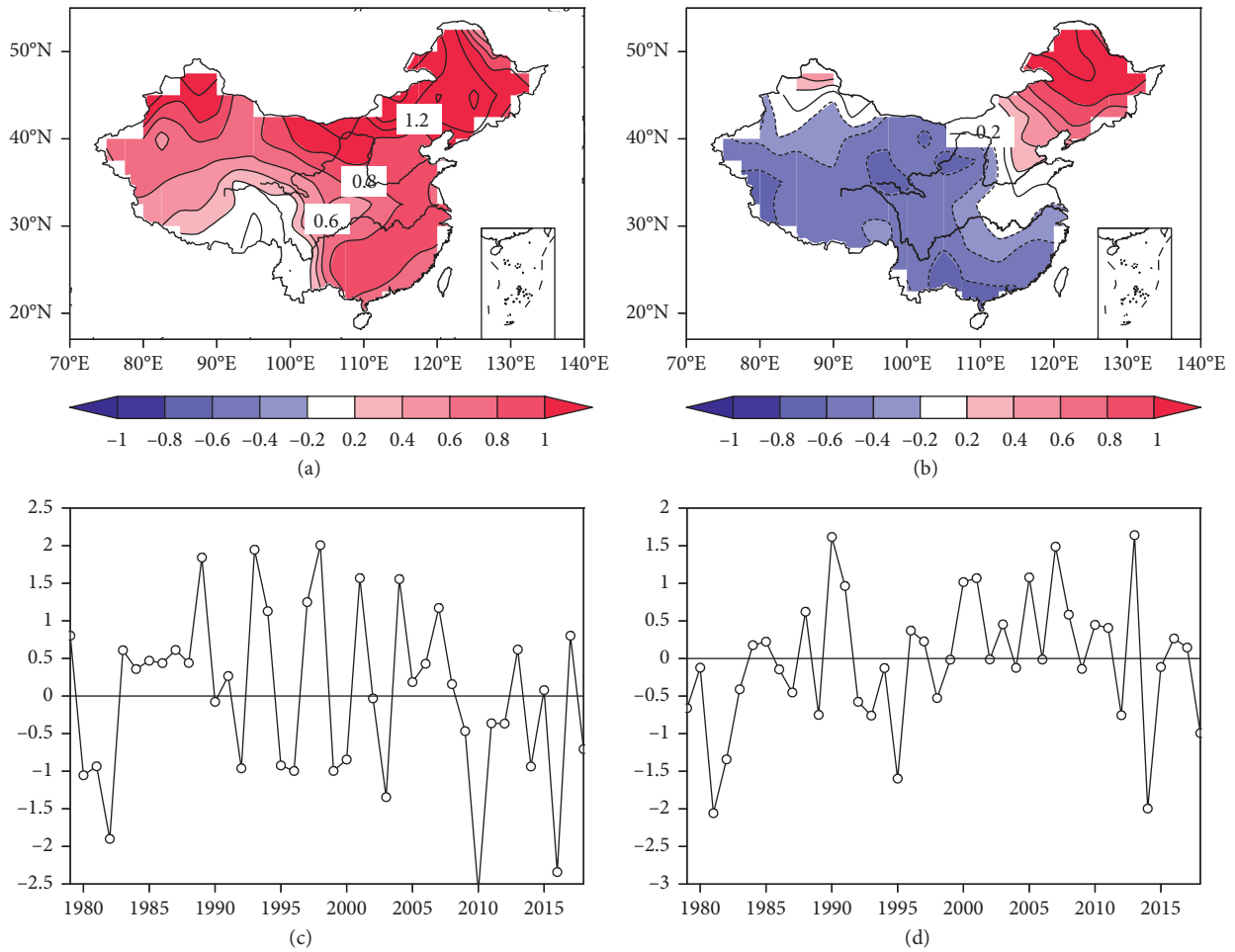

Figure 4: Spatial patterns of the first (a) and the second (b) EOF modes of the winter surface air temperature anomalies at 160 stations in China from 1979 to 2018 (unit: °C); the corresponding normalized time coefficients for the first (c) and the second (d) EOF modes.

Table 1: Correlation coefficients between the month-to-month detrended (original) BKI, ASI, PC1, and PC2.

EOF	BKI			ASI		
	9	10	11	9	10	11
PC1	**0.48*** (0.27)	**0.42*** (0.18)	0.19 (0.00)	**0.40*** (0.22)	**0.39** (0.29)	0.18 (0.23)
PC2	0.03 (−0.16)	0.18 (0.29)	**0.39** (**0.47***)	0.16 (**0.33**)	0.08 (0.27)	0.19 (**0.31**)

The bold font and asterisks indicate the significance exceeding 0.05 and 0.01, respectively.

correlations are indicated between PC2 and the sea ice cover in both the BK and the Arctic except for the BKI in November.

The above results show a decreasing relationship between the month-to-month variability of the BKI and the winter SAT in China, which suggests that more attention should be paid to the preceding September sea ice cover in the BK instead of the signals near October and November, which is when we focus on the seasonal prediction of winter SAT anomalies in China. Moreover, the detrended BKI time series presents a higher correlation than the original time series, implying that the interannual variability in the sea ice cover may play a more critical role in its association with the SAT in China compared with its linear trend component.

5. Sea Ice Loss-Associated Circulation

To explain how the preceding sea ice variation induces winter SAT anomalies in China, composite differences between the sea-level pressure (SLP) and the 850 hPa flow based on low-high OBKI (DBKI) values in September are presented in Figures 5(a) and 5(c). The difference field shows a positive anomalous winter pressure system in the northwestern part of the Eurasian continent that is suggestive of the northwestward expansion and intensification of the Cold Siberian High following the preceding loss of sea ice in the BK. Correspondingly, a massive anticyclone in the lower troposphere is present that is superimposed on the high-pressure system. This anomalous circulation pattern facilitates the invasion of cold air from high latitudes to East Asia

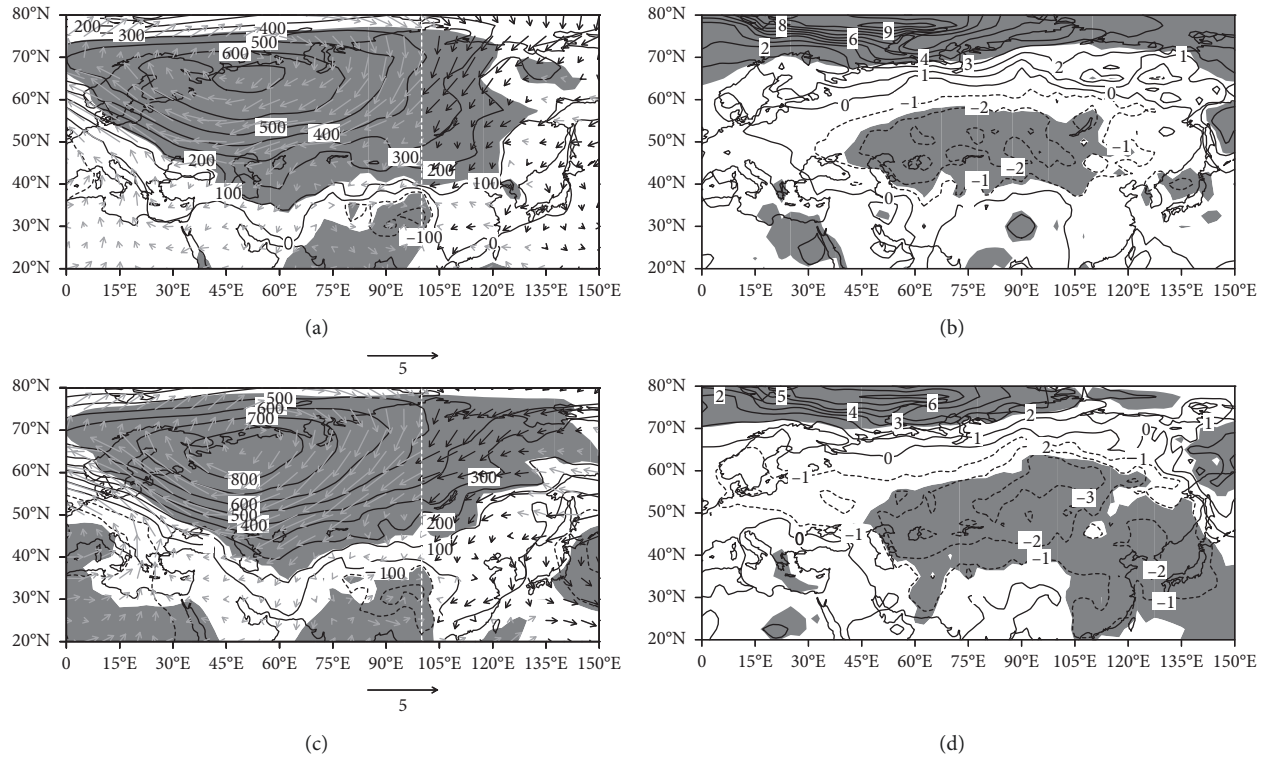

Figure 5: Composite differences for the (a) SLP (shaded and contour; unit: Pa), wind (vector; unit: m·s^{-1}) at 850 hPa, and (b) surface air temperature (shaded and contour; unit: ˚C) between selected low OBKI years and high OBKI years in September. (c, d) The same as (a) and (b) but for the composite differences between the selected low DBKI years and high DBKI years in September. The shading denotes significance exceeding 0.1. The black vectors indicate winds with a northerly component over the area east of 100˚E.

and the weakening of warm midlatitude westerlies from the North Atlantic that are instrumental to the cold advection. This corresponds to large areas of cold anomalies in the midlatitudes of Eurasia as well as East Asia (Figures 5(b) and 5(d)). Comparatively, the significant areas of the SAT between the low-high DBKI in September in Figure 5(d) extend more southeastward to the eastern part of China, the Korean Peninsula, Japan, and the Northwest Pacific than the DBKI in Figure 5(b). A substantial positive high-pressure system accompanied by a low-pressure system over the Northwest Pacific intensifies the land-sea pressure gradient. A northerly component correspondingly prevails in the area east of 100˚E on the Eurasian continent, which contributes to an intensification of the East Asian winter monsoon. However, the northerly component of the low-high OBKI is mainly present over the northeastern part of Eurasia. The associated response of the intensified East Asian winter monsoon to the low-high DBKI contributes to colder conditions in China compared with the response to the OBKI in September. Therefore, the following analysis is mainly based on the DBKI in September.

To explore the wintertime atmospheric response over Eurasia to the preceding variation of sea ice, we calculated the correlation coefficients between the DBKI in September and the circulation indices in winter. As shown in Table 2, most of the circulation indices are closely related to the September DBKI with significance exceeding 0.01 except for the AO index. In particular, the DBKI and the westerly index correlate positively with each other at 0.42, indicating favorable weakening westerly conditions and a meridional circulation pattern following the loss of sea ice in the BK. The significant anticorrelation between the blocking frequency, anticyclone intensity, and Siberian High index and the DBKI suggest that the retreat of the sea ice cover facilitates the maintenance and intensification of synoptic fluctuations, such as blocking highs and surface cold highs, which lead to an accumulated strengthening of the semipermanent Siberian High. Correspondingly, an increase in the land-sea pressure gradient over East Asia suggests an intensified East Asian monsoon that leads to large-scale cold anomalies in China. On the contrary, although the AO is well represented with the zonal mean status of midlatitude westerlies [38], the relationship of the westerly index with the DBKI is notably

Table 2: Correlation coefficients between the DBKI in September and the circulation indices in the winter.

Circulation indices	Correlation coefficient
Westerly index	**0.42**
Eurasian blocking high frequency	**−0.65**
Eurasian anticyclone intensity	**−0.55**
Siberian High intensity	**−0.45**
East Asian winter monsoon index	**−0.44**
AO index	0.21

The bold font indicates significance exceeding 0.01.

closer to the relationship between the AO and the DBKI. This implies a local connection of the preceding sea ice in the BK with the midlatitude climate anomalies. Kug et al. [14] also documented different local responses of the variations of the sea ice cover in the BK and in the East Siberian and Chukchi seas; the variation of the sea ice cover in the BK is associated well with the winter SAT anomalies over the Eurasian continent, while the variation of the sea ice cover in the East Siberian and Chukchi seas is mainly linked with the SAT anomalies over North America.

The reduction in sea ice has a direct connection to the warming of the air column and modifies the meridional thickness gradient over mid- to high-latitude regions, leading to the change in midlatitude weather [8, 12]. To examine the linkage between sea ice loss and midlatitude circulation, the regional means of the air temperature profiles over the BK (30°E–100°E, 75°N–85°N, referred to as the north region (NR)) and the midlatitudes of Eurasia (30°E–100°E, 40°N–50°N, referred to as the south region (SR)) were calculated, and their composite differences between low-high sea ice years are shown in Figure 6. A continuous warming in the NR from September (0 yr) to February (+1 yr) is indicated in the lower troposphere, but it decreases with an increase in the height (Figure 6(a)). Lower-troposphere warming is typically induced by the release of heat flux from the open ocean to the atmosphere due to the reduction in sea ice [39]. A clear difference in the warming in the NR is observed between the late autumn and winter. During October and November, the anomalous warming is mainly displayed below 850 hPa with a low significance, and a weak cooling can also be found in the upper air in November. However, substantial deep warming occurs in the midtroposphere and low troposphere in the winter with a maximum value of 3.2°C near the surface. Moreover, dominant cooling is evident in the SR, especially in January and February (Figure 6(b)). In addition, the September DBKI is associated more closely with midlatitude SAT variations in the winter than in the autumn. Furthermore, the composite differences of diabetic heating in the NR (SR) from December (0 yr) to February (+1 yr) between low-high sea ice years are 39.46 (9.04) w·m^{-2}, 34.14 (−9.55) w·m^{-2}, and 29.74(−7.68) w·m^{-2}, respectively. This suggests that the retreat of the sea ice in the BK in autumn favors the mid- and lower-tropospheric warming and thus weakens the meridional temperature between the high latitude and the midlatitude. The thermal conditions in the BK may play a driving role in the changes in the meridional temperature gradient and the associated thickness gradient.

6. Month-to-Month Oceanic Heat Storage Contrast and Associated Subsequent Warming

In this section, we will address the reason why the DBKI in September could be a better indicator of the SAT anomalies in China compared to the DBKI in the following October and November. As discussed above, the lower-troposphere air temperature in the BK shows clearly persistent warming from September to February and potentially results in a decrease of the meridional temperature gradient in the winter. Coincidently, the autumn heat content of the upper ocean in the BK presents a significantly warm difference between low and high DBKI (Figures 7(a)–7(c)). Moreover, a slightly warmer condition is induced by low-high September DBKI (S-DBKI) compared to the October DBKI (O-DBKI), and the contrast of oceanic warming is even more clear between the S-DBKI and the November DBKI (N-DBKI). The seasonal sea ice melting from May to September opens a large portion of the Arctic Ocean, allowing it to absorb sunlight during the warm season [40]. Therefore, the retreat of the autumn sea ice cover in the BK associates with more heat storage in the upper BK, especially in September. Correspondingly, the subsequent December-January mean surface sensible + latent heat flux and upward longwave radiation show a clear increase in the BK (Figures 7(d)–7(f)). The positive anomalous ocean-to-atmosphere energy indicates an additional release of oceanic heat storage in the BK to the atmosphere associated with the preceding low autumn sea ice cover. The winter heat anomalies in the BK and their surroundings are most pronounced to be associated with the S-DBKI compared to the O-DBKI and N-DBKI.

Figure 8 shows the composite differences between the December-January mean 500 hPa geopotential height (Z500) and the 850 hPa flow (V850) based on low-high DBKI values from September to November. A pronounced high Z500 center is shown in the BK and extends southward to the Ural Mountains associated with low S-DBKI (Figure 8(a)). Similar Z500 anomaly patterns also present through the whole troposphere with a barotropic vertical structure (figure not shown) and link with the amplification tropospheric warming induced by sea ice loss. Furthermore, the anomalous southerlies from the high latitudes of Northern Atlantic drive warm advection into the BK and facilitate a further amplification warming. The warming over the BK links with the release of oceanic heat storage to the atmosphere and associated anomalous warm advection over the Barents Sea and cold advection over the midlatitude of the Eurasia. A notable difference in temperature between the BK and the midlatitude of Eurasia results in the significant weakened meridional temperature gradient. This decelerates the westerlies and leads to more active surface anticyclone and blocking (Table 2) and anticyclonic vorticity forcing to their north [41]. Correspondingly, large-scale anticyclonic circulation is shown over the northwest of Eurasia. As discussed in Section 5, the anomalous anticyclonic circulation over the Ural Mountains and BK leads to more Ural blocking, a deeper East Asian trough, and more intense cold air invasion into the East Asian region. In contrast, the low O-DBKI and N-DBKI associated Z500 anomalies display a northwestward-displaced positive center over the west of Greenland (Figures 8(b) and 8(c)). Cold advection from the east Siberian sector of Arctic is weaker compared to S-DBKI-associated Z500 anomalies (Figure 8(a)). Consequently, the S-DBKI shows a higher correlation with winter SAT anomalies in China.

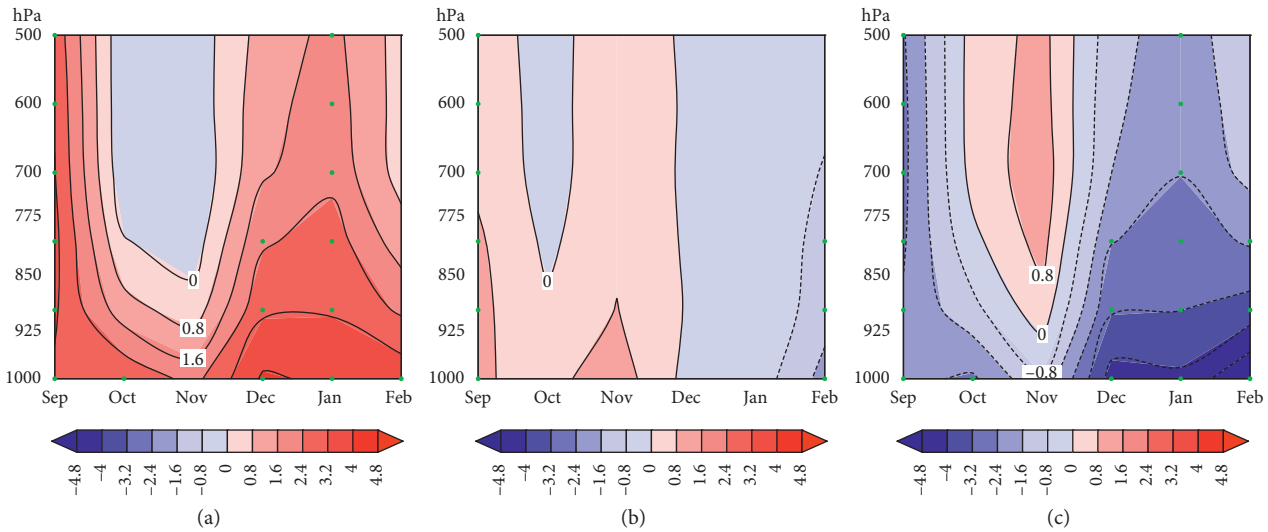

FIGURE 6: Composite differences for (a) vertical profiles of the temperature (shaded; unit: °C) in the BK region/NR (30°E–100°E, 75°N–85°N) from September to the following February between selected low DBKI years and high DBKI years in September. (b, c) The same as (a) but for the midlatitude region/SR (30°E–100°E, 40°N–50°N) and the differences between the SR and the NR, respectively. The green dot denotes the values that are statistically significant with significance exceeding 0.1 based on the results of *t*-tests.

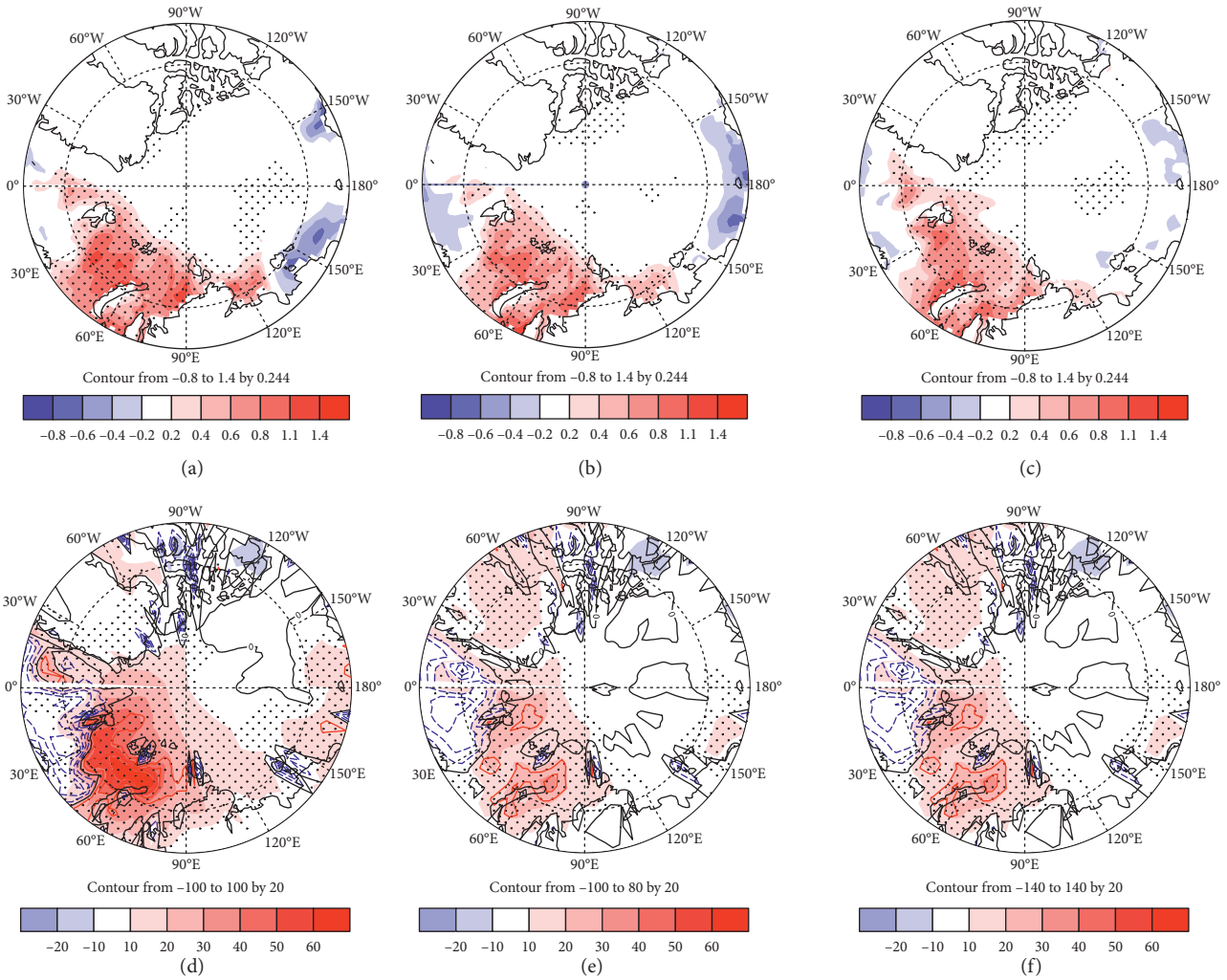

FIGURE 7: Composite differences for the SON mean upper ocean heat content (shaded) between selected low and high DBKI in September (a), October (b), and November (c) (unit: K). (d–f) The same as (a), (b), and (c) but for DJF mean upward longwave radial (shaded) and sensible + latent heat flux (contour) (unit: $w \cdot m^{-2}$). The dotted areas denote the values that are statistically significant with significance exceeding 0.1 based on the results of *t*-tests for heat content in (a), (b), and (c) and longwave radiation in (d), (e), and (f).

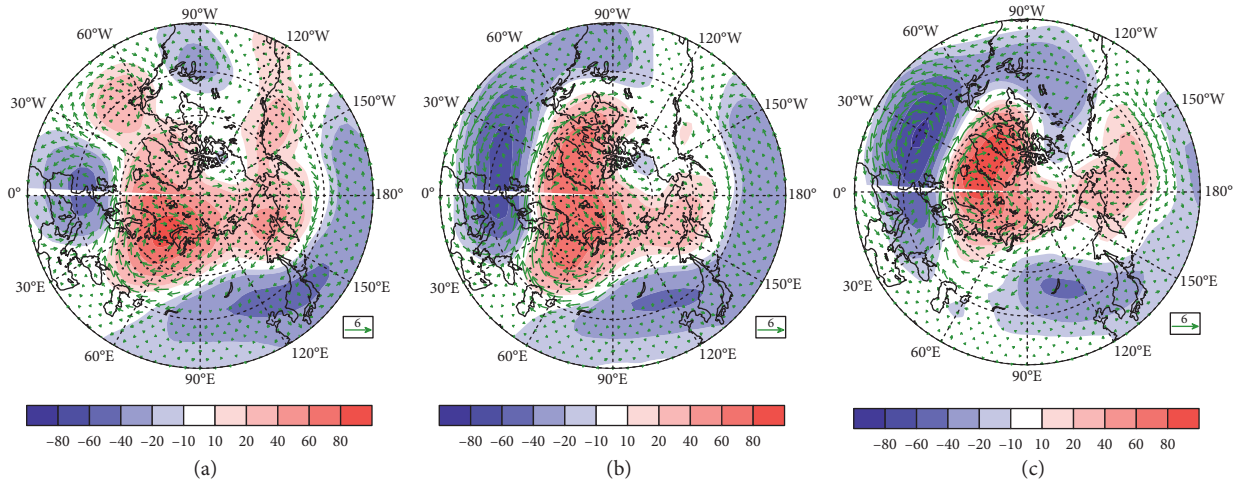

Figure 8: The same as (d), (e), and (f) in Figure 7 but for DJF mean Z500 (shaded) (unit: gpm) and V850 (vector) (unit: m·s^{-1}). The dotted areas denote the values that are statistically significant with significance exceeding 0.1 based on the results of *t*-tests for Z500.

7. Conclusions

The variation of the autumn Arctic sea ice area and the relationship between the month-to-month sea ice and the winter temperature anomalies in China are investigated in this study. The conclusions based on the main results are as follows:

(1) The sea ice cover in the BK during the autumn season has shown a substantial decrease during the past three decades. The region of accelerating sea ice reduction since 2005 agrees well with the Arctic superimposed with a large interannual variability.

(2) The retreat of autumn sea ice in the BK is significantly associated with large-scale negative temperature anomalies in the following winter in China, and this retreat correlates well with the dominant sign-consistent SAT mode (EOF1) in China, except for the Tibetan Plateau. However, the ice-SAT lag correlation shows a notable month-to-month diversity in which the linkage between the sea ice in the BK in September and the winter temperature is stronger than that in both October and November. Moreover, the detrended sea ice cover in the BK as a potential predictor is associated more closely with the SAT in China than the original sea ice cover in the BK.

(3) An anomalous positive surface pressure is exhibited over the northwestern part of Eurasia in the winter that is linked to the decreasing sea ice in the BK region in the preceding September. This surface pressure favors the persistence and intensification of synoptic perturbations, such as blocking highs and surface cold highs, as well as the intensification of the Siberian High and East Asian winter monsoon. These favorable conditions ultimately contribute to the formation of large-scale winter cold anomalies in China.

(4) Compared to low O-DBKI and N-DBKI, a more oceanic heat storage in the upper BK is induced by low S-DBKI leading to a larger heat release to tropospheric atmosphere by surface heat flux in the BK. This regional tropospheric warming results in a higher barotropic positive height anomaly over the Ural Mountains, and thus, more active cold advection from the high latitude affects East Asia.

Data Availability

The data used to support the findings of this study are included within the article: (1) the European Centre for Medium-Range Weather Forecasts (ECMWF) reanalysis dataset (ERA-Interim) from 1979 to 2018 is used for deriving data on the daily and monthly air temperatures, sea-level pressure, geopotential height, and horizontal wind; (2) monthly mean sea ice concentrations are derived from the Met Office Hadley Centre's sea ice and sea surface temperature (HadiSST 1.1) dataset; (3) the monthly mean heat content is derived from the vertical average of potential temperature (109.8 m above; 11 levels) from the ECMWF ocean reanalysis system ORAS4; and (4) observed monthly mean surface air temperatures (SATs) are from the National Climate Center of China, including 160 stations.

Conflicts of Interest

The authors declare that there are no conflicts of interest regarding the publication of this paper.

Acknowledgments

This work was supported jointly by the National Basic Research Program of China (Grant no. 2015CB953904) and the National Natural Science Foundation of China (Grant nos. 41975073, 41575081, and 41741005).

References

[1] T. R. Karl, A. Arguez, B. Huang et al., "Possible artifacts of data biases in the recent global surface warming hiatus," *Science*, vol. 348, no. 6242, pp. 1469–1472, 2015.

[2] X. Zhang, C. Lu, and Z. Guan, "Weakened cyclones, intensified anticyclones and recent extreme cold winter weather events in Eurasia," *Environmental Research Letters*, vol. 7, no. 4, Article ID 044044, 2012.

[3] C. H. Lu, S. Q. Xie, Y. J. Qin et al., "Recent intensified winter coldness in the mid-high latitudes of Eurasia and its relationship with daily extreme low temperature variability," *Advances in Meteorology*, vol. 2016, Article ID 3679291, 11 pages, 2016.

[4] L. Yang and B. Wu, "Interdecadal variations of the East Asian winter surface air temperature and possible causes," *Chinese Science Bulletin*, vol. 58, no. 32, pp. 3969–3977, 2013.

[5] L. Wang and W. Chen, "The East Asian winter monsoon: Reamplification in the mid-2000s," *Chinese Science Bulletin*, vol. 59, no. 4, pp. 430–436, 2014.

[6] J. A. Francis, "Why are Arctic linkages to extreme weather still up in the air?," *Bulletin of the American Meteorological Society*, vol. 98, no. 12, pp. 2551–2557, 2017.

[7] J. Overland, "Potential arctic change through climate amplification processes," *Oceanography*, vol. 24, no. 3, pp. 176–185, 2011.

[8] J. A. Francis and S. J. Vavrus, "Evidence linking Arctic amplification to extreme weather in mid-latitudes," *Geophysical Research Letters*, vol. 39, no. 6, Article ID L06801, 2012.

[9] B.-M. Kim, S.-W. Son, S.-K. Min et al., "Weakening of the stratospheric polar vortex by Arctic sea-ice loss," *Nature Communications*, vol. 5, no. 1, 2014.

[10] E. A. Barnes, "Revisiting the evidence linking Arctic amplification to extreme weather in midlatitudes," *Geophysical Research Letters*, vol. 40, no. 17, pp. 4734–4739, 2013.

[11] C. Deser and H. Teng, "Evolution of Arctic sea ice concentration trends and the role of atmospheric circulation forcing 1979–2007," *Geophysical Research Letters*, vol. 35, no. 2, Article ID L02504, 2008.

[12] J. E. Overland and M. Wang, "Large-scale atmospheric circulation changes are associated with the recent loss of Arctic sea ice," *Tellus A: Dynamic Meteorology and Oceanography*, vol. 62, no. 1, pp. 1–9, 2010.

[13] M. Mori, M. Watanabe, H. Shiogama, J. Inoue, and M. Kimoto, "Robust Arctic sea-ice influence on the frequent Eurasian cold winters in past decades," *Nature Geoscience*, vol. 7, no. 12, pp. 869–873, 2014.

[14] J. S. Kug, J. H. Jeong, Y. S. Jang et al., "Two distinct influences of Arctic warming on cold winters over North America and East Asia," *Nature Geoscience*, vol. 8, no. 10, Article ID NGEO2517, pp. 759-762, 2015.

[15] P. Ruggieri, R. Buizza, and G. Visconti, "On the link between Barents-Kara sea ice variability and European blocking," *Journal of Geophysical Research: Atmospheres*, vol. 121, no. 10, pp. 5665–5679, 2015.

[16] Z. Lü, S. He, F. Li, and H. Wang, "Impacts of the autumn Arctic sea ice on the intraseasonal reversal of the winter Siberian High," *Advances in Atmospheric Sciences*, vol. 36, no. 2, pp. 173–188, 2019.

[17] Q. Xie and S. S. Huang, "Study of influence of equatorial SST over Mid-East Pacific ocean and Arctic sea-ice anomalies to general circulation," *Scientia Meteorologica Sinica*, vol. 10, no. 4, pp. 325–338, 1990.

[18] B. Wu, D. Gao, and R. Huang, "ENSO events and interannual variations of winter sea-ice in the Greenland, the Kara and the Barents Seas," *Chinese Science Bulletin*, vol. 42, no. 16, pp. 1382–1385, 1997.

[19] X. Q. Yang, Q. Xie, and S. S. Huang, "Modelling influence of Arctic sea-ice anomalies to Asian summer monsoon," *Acta Meteorologica Sinica*, vol. 16, no. 4, pp. 34–40, 1994, in Chinese.

[20] X. M. Shi, Y. W. Sun, and J. L. Sun, "The impact of zonal temperature gradient in the Arctic Ocean on the summer precipitation over Northeast China," *Periodical of Ocean University of China*, vol. 44, no. 2, pp. 11–16, 2014, in Chinese.

[21] H. J. Wang, H. P. Chen, and J. Liu, "Arctic sea ice decline intensified haze pollution in Eastern China," *Atmospheric and Oceanic Science Letters*, vol. 8, no. 1, pp. 1–9, 2015.

[22] B. Y. Wu, R. H. Huang, and D. Y. Gao, "The impact of variation of sea-ice extent in the Kara Sea and the Barents Seas in winter on the winter monsoon over East Asia," *Chinese Journal of Atmospheric Sciences*, vol. 23, no. 3, pp. 267–275, 1999, in Chinese.

[23] X. H. Xie and X. Q. Yang, "Interannual relationship between Arctic sea ice concentration anomaly and China air temperature variation during winter," *Journal of Nanjing University (Natual Sciences)*, vol. 42, no. 6, pp. 549–561, 2006.

[24] B. Y. Wu, J. Z. Su, and R. H. Zhang, "Effects of autumn-winter Arctic sea ice on winter Siberian High," *Chinese Science Bulletin*, vol. 56, no. 30, pp. 3220–3228, 2011.

[25] F. Li, H. J. Wang, and Y. Q. Gao, "Change in sea ice cover is responsible for non-uniform variation in winter temperature over East Asia," *Atmospheric and Oceanic Science Letters*, vol. 8, no. 6, pp. 376–382, 2015.

[26] C. Y. Zhu, F. Huang, Y. H. Shi et al., "Spatial-temporal patterns of the cold surge events in China in recent 50 years and its relationship with Arctic sea ice," *Periodical of Ocean University of China*, vol. 44, no. 12, pp. 12–20, 2014, in Chinese.

[27] C. Li and Q. Zhang, "January temperature anomalies over Northeast China and precursors," *Chinese Science Bulletin*, vol. 58, no. 6, pp. 671–677, 2013.

[28] D. W. Wang and X. Q. Yang, "Temporal and spatial patterns of Arctic sea ice variations," *Acta Meteorologica Sinica*, vol. 60, no. 2, pp. 129–138, 2002.

[29] J. H. He, F. M. Wu, and L. Qi, "Decadal/interannual linking between autumn Arctic sea ice and following winter Eurasian air temperature," *Chinese Journal of Geophysics*, vol. 58, no. 4, pp. 1089–1102, 2015, in Chinese.

[30] D. P. Dee, S. M. Uppala, A. J. Simmons et al., "The ERA-Interim reanalysis: configuration and performance of the data assimilation system," *Quarterly Journal of the Royal Meteorological Society*, vol. 137, no. 656, pp. 553–597, 2011.

[31] N. A. Rayner, D. E. Parker, and E. B. Horton, "Global analyses of sea surface temperature, sea ice, and night marine air temperature since the late nineteenth century," *Journal of Geophysical Research*, vol. 108, no. D14, 2003.

[32] M. A. Balmaseda, K. Mogensen, and A. T. Weaver, "Evaluation of the ECMWF ocean reanalysis system ORAS4," *Quarterly Journal of the Royal Meteorological Society*, vol. 139, no. 674, pp. 1132–1161, 2013.

[33] D. Y. Gong and C. H. Ho, "The Siberian High and climate change over middle to high latitude Asia," *Theoretical and Applied Climatology*, vol. 72, no. 1-2, pp. 1–9, 2002.

[34] J. G. Charney, J. Shukla, and K. C. Mo, "Comparison of a barotropic blocking theory with observation," *Journal of the Atmospheric Sciences*, vol. 38, no. 4, pp. 762–779, 1981.

[35] N. Shi and Y. S. Yang, "Main characteristics of east Asian summer/winter intermonsoon index for 1873~1996," *Journal of Nanjing Institute of Meteorology*, vol. 21, no. 2, pp. 208–214, 1998, in Chinese.

[36] J. Inoue and E. H. Masatake, "The role of Barents sea ice in the wintertime cyclone track and emergence of a warm-Arctic

cold-Siberian anomaly," *Journal of Climate*, vol. 25, no. 7, 2012.

[37] G. R. North, T. L. Bell, R. F. Cahalan, and F. J. Moeng, "Sampling errors in the estimation of empirical orthogonal functions," *Monthly Weather Review*, vol. 110, no. 7, pp. 699–706, 1982.

[38] D. W. J. Thompson and J. M. Wallace, "Annular modes in the extratropical circulation. Part I: month-to-month variability," *Journal of Climate*, vol. 13, no. 5, pp. 1000–1016, 2000.

[39] J. A. Screen and I. Simmonds, "The central role of diminishing sea ice in recent Arctic temperature amplification," *Nature*, vol. 464, no. 7293, pp. 1334–1337, 2010.

[40] A. Dai, D. Luo, M. Song et al., "Amplification is caused by sea-ice loss under increasing CO_2," *Nature Communications*, vol. 10, no. 121, pp. 1–13, 2019.

[41] N.-C. Lau, "Variability of the observed midlatitude storm tracks in relation to low-frequency changes in the circulation pattern," *Journal of the Atmospheric Sciences*, vol. 45, no. 19, pp. 2718–2743, 1988.